Fourth Australian Conference on Laser Diagnostics in Fluid Mechanics and Combustion
The University of Adelaide, South Australia, Australia
7-9 December 2005

Joint Imaging of Rayleigh and LIF-OH at the Base of Lifted Flames Issuing in Vitiated Coflow

R. L. Gordon, M. J. Dunn, A. R. Masri, and R. W. Bilger

School of Aerospace, Mechanical and Mechatronic Engineering,
The University of Sydney, N.S.W. 2006, AUSTRALIA
robert.gordon@aeromech.usyd.edu.au

ABSTRACT

The stabilisation of a lifted flame issuing in a vitiated co-flow has been studied both experimentally and numerically with the objective of resolving whether the dominant mechanism is due to auto-ignition or to premixed flame propagation. A key parameter used in both studies is the lift-off height, L_H defined at the first location of occurrence of heat release downstream of jet exit plane. Experimentally, L_H is either observed visually or obtained from direct photographs of the flame. Numerically, L_H is obtained from the profiles of temperature or reactive scalar such as the hydroxyl radical OH.

This paper presents measurements of temperature and the hydroxyl radical, OH made at the base of lifted flames using joint Rayleigh-LIF-OH imaging. Temperature is deduced from Rayleigh imaging while the quenching correction for OH is applied using correlations generated, as functions of temperature, from opposed flow flame calculations. These measurements form a sound platform for comparison with calculations. Also, the images may highlight differences in the flame structure depending on whether stabilisation is due to auto-ignition or premixed flame propagation.

1. INTRODUCTION

The lifted turbulent jet flame is an interesting and important topic in turbulent combustion. Various theories for the mechanism of stabilization of such flames have been comprehensively reviewed by Pitts [1]. That proposed by Vanquickenborne and van Tiggelen [2] argues that flame stabilization occurs at the position where the axial mean velocity balances the turbulent burning velocity for entirely premixed conditions. The theory suggested by Peters and Williams [3], argues that diffusion flame propagation will proceed along instantaneous surfaces of stoichiometric mixture up to the position where too many flamelets are quenched, so that flame propagation of the turbulent flame towards the nozzle cannot proceed further. Recently, measurements of detailed single point data as well as planar images of a range of scalars have been made near the flame stabilization region of turbulent lifted jet flames [4, 5, 6]. The results indicate that the phenomenon may be more complicated and continues to pose a challenge to the understanding of the stabilization mechanism.

Practical burners achieve stabilization by recirculation of hot combustion products. A vitiated coflow burner developed by Cabra et al [7] enables investigation of stabilization mechanisms in an environment that decouples the turbulent chemical kinetics from the complex recirculating flow. The vitiated coflow is a large pilot that provides a uniform environment for the investigation of highly turbulent jet flames with low Damköhler numbers. Due to the hot coflow of combustion products, auto-ignition of the fuel mixture can occur downstream, thus the stabilization mechanism in a vitiated coflow can be different from flames stabilized in cool air.

An advantage of the Cabra burner is that issues of auto-ignition in a turbulent flow as well as the mechanism of lift-off stabilization can be investigated in a simple, well-defined turbulent flow with excellent optical access, and in a setup that is conducive to modeling. Some calculations of these flames have already appeared in the literature [7, 8]. Measurements of lift off heights are based on visible images of the flame base while calculations use the increase in hydroxyl concentrations to mark the reaction zone. Differences between these markers may distort the comparisons.

This paper presents simultaneous quantitative images and data of temperature and the hydroxyl radical, OH, taken near the mean flame base of methane lifted flames at several lift-off heights. Mean data have been generated to form a database for comparisons to numerical work, and several instantaneous images are presented to examine for potential differences in the stabilisation mechanism at different lift-off heights

2. EXPERIMENTAL SETUP

The same burner setup described in Wu et al. [9], is used in all these measurements. This is a replica of the vitiated coflow burner in combustion analysis lab of U.C. Berkeley [7]. The burner [7, 10] consists of a central jet (H_2/N_2 or Methane/Air) flame in a coaxial flow of hot combustion products from lean premixed H_2/Air flames (vitiated coflow). The coflow diameter is 198 mm, and the central nozzle with an inner diameter D = 4.45 mm extends 70 mm above the perforated plate surface. The methane fuel jet is a mixture of 33% CH4 and 67% Air (molar). The velocities of the jet and the coflow are determined from the mixture density and flow rates.

The experimental setup is shown in Figure 1. The Rayleigh laser was generated from the second harmonic of a SpectraPhysics Pro350 Nd:YAG, operating at an energy of 130mJ/pulse. The resulting 2-D sheet that was formed was 25mm high. The 283.2 nm UV beam at 28mJ/Pulse for the OH-LIF was generated from the frequency doubling of a Syrah Pumped Dye Laser (PDL) using Rhodamine 6G in ethanol, pumped by the second harmonic of a seeded SpectraPhysics Pro350 Nd:YAG.

There is no significant beam steering in the coflow, where density gradients are very low.

The experimental parameters of coflow and fuel jet velocity (5.3 m/s and 100 m/s respectively), match the conditions of the methane flame of Cabra [7]. Coflow temperature has been varied to attain lift-off heights of 25, 35 and 40 x/D.

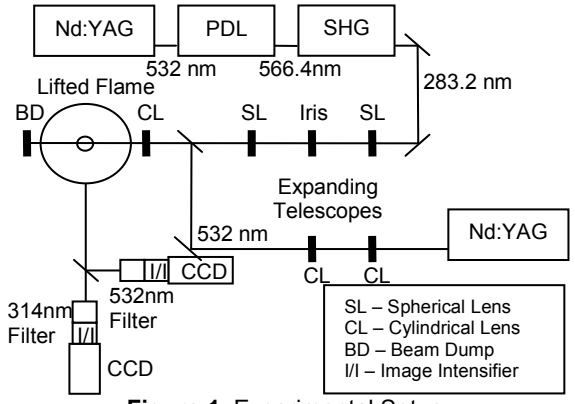

Figure 1. Experimental Setup.

3. IMAGE PROCESSING

3.1 Rayleigh image processing

The procedure for the derivation of quantitative images for temperature is thoroughly detailed in Dunn et al [11]. In this paper, a simplifying assumption that the laser shot noise is equal to the average laser power, as the shot to shot noise is less than 2% of laser power. Assuming constant atmospheric pressure and ideal gasses, equation (1) can be used to relate the molecular number density to the temperature of the flame:

$$\frac{T_{Flame}}{T_{Air}} = \frac{\left(\sum_{i=1}^{j} X_i \sigma_i\right)_{flame} I_{Rayleigh,Air}}{\sigma_{Air} I_{Rayleigh,Flame}} \qquad (1)$$

X_i is the mole fraction of species i and σ_i is the cross section for species i. $I_{Rayleigh,\ Air}$ and $I_{Rayleigh,\ Flame}$ are the captured response images, and σ_{Air} is the Rayleigh cross-section of air. The only unknown that remains in equation (1) is the flame shot cross section.

Data from 1D laminar and strained opposed flow simulations with the open source Cantera code (Goodwin [12]) was used to evaluate the variation of cross section with respect to temperature. For these simulations the equilibrium composition of the coflow combustion products is used for one stream and the composition of the central jet used for the other.

A number of strain rates were evaluated and the change cross section with respect to temperature was approximated with the quadratic (2):

$$\sigma = 1.259 \times 10^{-7} T^2 - 5.481 \times 10^{-4} T + 1.609 \quad (2)$$

which is graphed in Figure 2. The actual Rayleigh cross-section calculated from the laminar opposed flow case is shown for reference.

Tests of this method in the post-flame gasses of a Hencken Burner in diffusion mode running a stoichiometric methane-air mix indicate that the uncertainty in the temperature measurements are in the order of 10%.

Of note in Figure 2 is that the quadratic introduces a known error in the evaluation of the cross-section of around 8% in the temperature range 1000K to 1600K. Cold (fuel) gas temperatures will be understated and hot coflow gasses (the lower part of the curve) will be overstated.

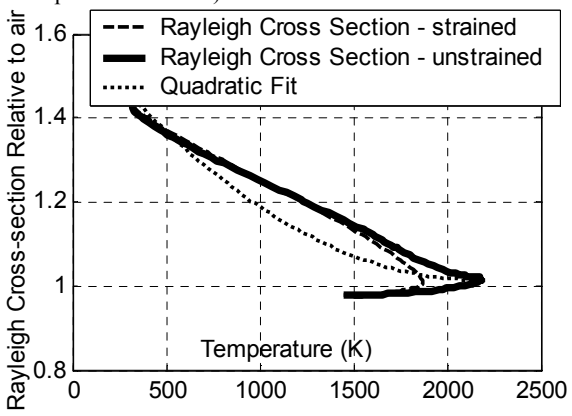

Figure 2. Variation of Rayleigh cross-section vs Temperature.

3.2 OH Fluorescence image processing

We assume a four level model (Daily [13]) for the OH molecule for $Q_1(7)$ excitation of the $A^2\Sigma^+$-$X^2\Pi$ (1,0) system. The derivation of the processing can be found in Dunn et al [11], with the following relevant notes. The mole fraction of OH X_{OH} may be expressed as:

$$X_{OH} = \frac{\eta_{OH} F_{OH} \tau_3^{-1} \tau_4^{-1}}{I_{Laser} B_{14} f_B(J'') \left(\frac{PN_a}{R_u T}\right)\left(\tau_3^{-1} A_{42} + A_{31} V_{43}\right)} \qquad (3)$$

η_{OH} represents the OH collection system throughput efficiency, F_{OH} is the dark noise corrected Fluorescence signal, τ_4^{-1} and τ_3^{-1} are the decay rates of populations of N_4 and N_3 respectively, I_{laser} is the laser photon density, B_{14} is the Einstein absorption rate of the laser coupled ground state. $f_B(J'')$ is the Boltzmann fraction in the laser coupled rotational level J'' of the electronic ground state. A_{42}, and A_{31} are the net spontaneous emission rates from v'=1 to v''=1, and v'=0 to v''=0 respectively. V_{43} is the vibrational transfer rate from v'=1 to v'=0. P is the pressure, N_a is Avogadro's number, R_u the universal gas constant and T the corresponding temperature from the processed Rayleigh image.

Of particular interest from equation (3) is that with the proposed fluorescence model the fluorescence intensity displays an asymptotically correct relationship with the laser photon density, I_{laser}.

In order to evaluate the electronic quenching rates from the excited $A^2\Sigma^+$ v'=1 and v'=0 levels, experimentally derived data for the two species-dependant constants and the species quenching cross-sections needs to be generated. The generation of the quenching and vibrational transfer rates is numerically identical to that used in Dunn et al [11].

As with the Rayleigh processing, variation of the quenching rates with temperature has been simulated for a variety of strain rates in a 1D opposed flow diffusion flame. From these, quadratic relations of best fit were developed (Equations 4, 5). The temperature is taken from the corresponding processed Rayleigh image.

$$V_{43} = 7 \times 10^2 T^2 - 2.7 \times 10^6 T + 6.3 \times 10^9 \qquad (4)$$

$$Q_{3,4} = 6.5 \times 10^2 T^2 - 6.8 \times 10^5 T + 2.9 \times 10^9 \qquad (5)$$

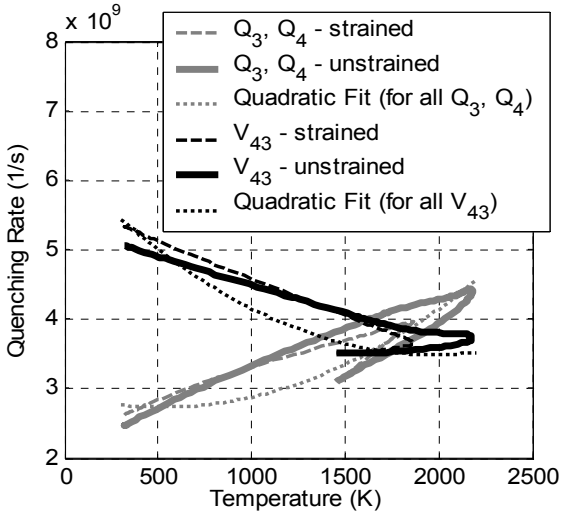

Figure 2. Variation of Quenching Rate with Temperature. Quadratic fits are best fit over all cases.

Tests of this method in the post-flame gasses of a Hencken Burner discussed earlier indicate that the uncertainty in the OH measurements is in the order of 50%.

4. RESULTS

4.1 Mean Radial Profiles

Mean profiles were calculated from groups of 100 images at an axial location of 35 diameters. These are compared with point data taken at U.C. Berkeley. The flame studied by Cabra et al exhibited a liftoff height of 35 D. The 1380K coflow flame here lifts off just downstream of 35 diameters, the 1400K coflow flame lifts off around 32 diameters, and the 1420K coflow flame around 27 diameters.

The centreline temperatures (Figure 3) appear to be exaggerated, although they are not unreasonable given the uncertainty in the method. The OH profiles correspond to our understanding that no significant combustion should be seen in the 1380K coflow flame, whereas the other two flames should exhibit established mean flame bases or diffusion flame fronts. The radial location of the flame matches well with previous data [7].

The mean OH concentrations and temperature rises goes some way to confirming that OH is a valid lift-off height marker for this flame series. Of added interest in understanding the nature of the stabilisation region of these flames is the flame structure information gained from the instantaneous images.

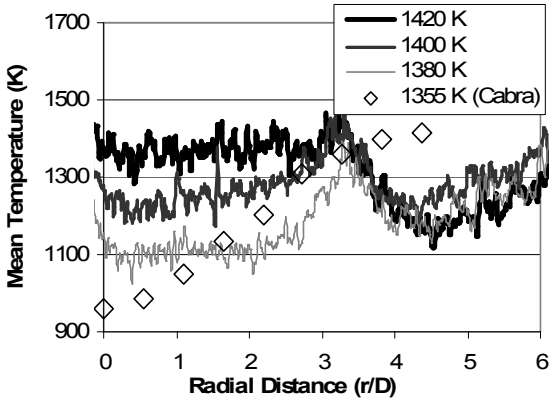

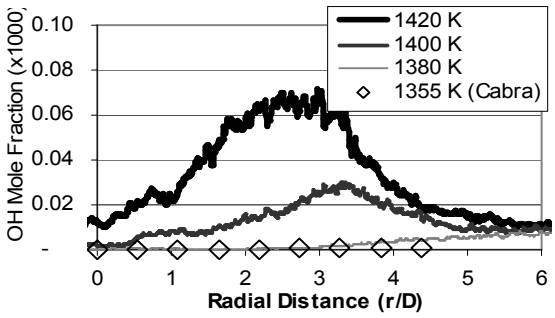

Figure 3. Radial profiles at x/D = 35 for coflow temperatures of approximately 1380K, 1400K and 1420K. Point measurements of Cabra (coflow temperature 1355K) are also included.

4.2 Instantaneous Images

A selection of quantitative instantaneous temperature and OH mole fraction images appears below in Figures 4 through 7., taken at x/D = 35. In each pair, the top image is OH mole fraction, the bottom image is Rayleigh temperature. The image domains extend radially from -6.4 r/D to 0 r/D, and +/- 1.75 diameters axially.

One of the goals of this series of experiments is to gain greater understanding of the nature of the flame at the mean flame base. Whether these flames are stabilised through autoignition events, flame propagation into a partially premixed fluid, or some more complex mechanism is still unanswered. It is possible that autoignition kernels could be captured in planar imaging as regions of OH that are not attached to the leading edge of a flame front. However, one of the limitations of single sheet imaging is that no data is captured regarding non-orthogonal aspects of this flame. It is possible that this aspect exists at axial locations 35 diameters downstream

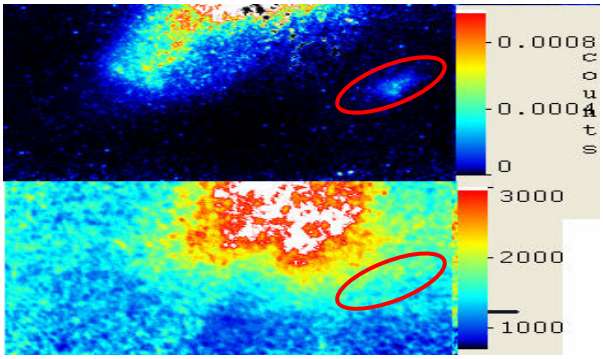

Figure 4. 1380K coflow, x/D = 35.

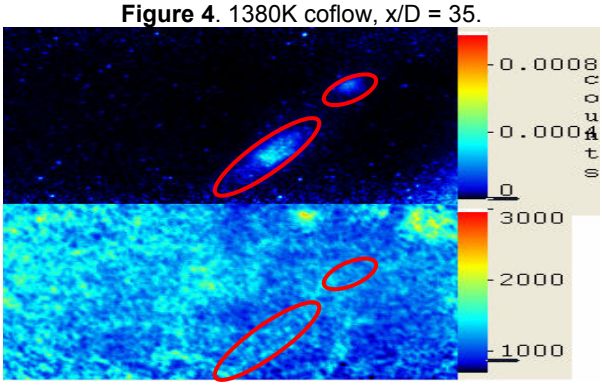

Figure 5. 1400K coflow, x/D = 35.

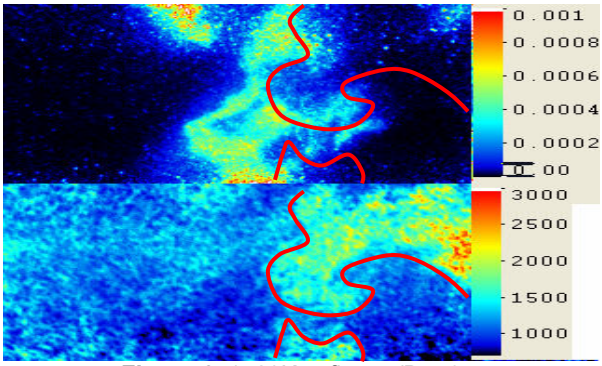

Figure 6. 1420K coflow, x/D = 35.

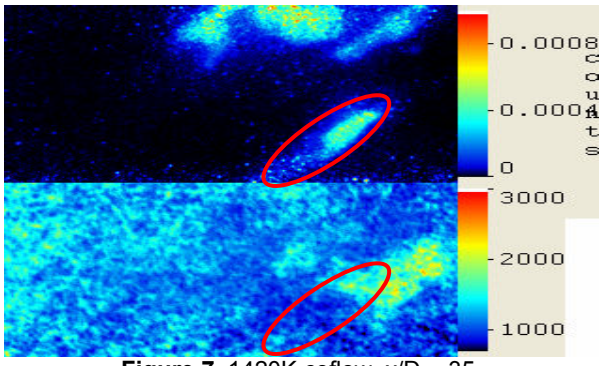

Figure 7. 1420K coflow, x/D = 35.

Figure 4 shows the one of few flame events captured at this location for the 1380K coflow flame. There exists an OH kernel near the centerline (marked with a red oval) that does not yet have an associated temperature rise. This could be an autoignition event, or an azimuthal projection into the laser sheet that may be linked to the region of hot gasses downstream.

In the 1400K case (Figure 5), flame events occurred with greater frequency, but events such as the one captured here still highlight the possibility of autoignition several diameters above the mean flame base.

The majority of the flame events in the 1420K coflow flame appeared to be developed diffusion jet flames, with an OH band lying at the fuel-oxidiser interface, and the hot gas region lying on the rich side of the interface, such as Figure 6, where the red contour highlights the edge of the hot gas region, and is overlayed on the OH image. However, images such as Figure 7 also show a highly turbulent flame, possibly with local extinction (above the OH event marked with an oval).

Subsequent to this serries of experiments, the Rayleigh image quality has been greatly improved. The "graininess" in these images was a feature of the intensifier used, which is no longer part of the setup. The entire optics chain has been redesigned, and pixel binning has been employed to improve signal-to-noise ratio. Further work will be undertaken to improve the OH image quality, and the calibration data.

The non-orthogonality aspect of the flame could be investigated using a double-sheet LIF method.

5. CONCLUSIONS

Quantitative simultaneous planar Rayleigh temperature and OH-LIF images have been generated for lifted flames in a vitiated coflow. Temperature is deduced from Rayleigh imaging. A relationship for mole fraction of OH was used that is valid through the linear and saturation regions of fluorescence for OH, and the quenching correction for OH is applied using correlations generated, as functions of temperature, from opposed flow flame calculations.

The mean data matches well with previous experimental studies, except near the centreline of the flame. Improvements in the optics and calibration will further improve the results from this experimental setup. While the curve-fit method for obtaining the Rayleigh Cross Section and quenching factors introduces systematic error into the processing, it worth noting that the bounds on these values established from unstrained and strained 1-D flame calculations are well constrained.

Instantaneous imaging of the mean flame base indicates possible autoignition events as a stabilisation mechanism, and these events seem to exist even deeper axially into the flame. It is not yet possible, however, to draw conclusions from this as other effects could be at work, such azimuthal projections of OH into the laser sheet.

ACKNOWLEDGMENTS

This research is supported by the Australian Research Council.

REFERENCES

[1] Pitts, W.M., *Proceedings of the Combustion Institute* **22**, 1988, 809-816.

[2] Vanquickenborne, L. and Van Tiggelin, A., *Combustion and Flame* **10,** 1966, 59–69.

[3] Peters, N. and Williams, F.A., *AIAA Journal,* **21,** 1983, 423–429.

[4] Stårner, S.H., Bilger, R.W., Frank, J.H, Marran, D.F. and Long, M.B., *Combustion and Flame* **107,** 1996, 307–313.

[5] Kelman J. B., Eltobaji A. J., and Masri A. R., *Combustion Science and Technology,* **135,** 1998, 117-134.

[6] Upatnieks, A., Driscoll, J. F., and Ceccio, S. L., *Proceedings of the Combustion Institute* **29**, 2002, 1897-1904.

[7] Cabra R., Myhrvold T., Chen J.Y., Dibble R.W., Karpetis A. N. and Barlow R. S., *Proceedings of the Combustion Institute,* **29**, 2002, 1881-1888.

[8] Masri A.R., Cao R., Pope S.B., and Goldin G.M., *Combustion Theory and Modeling*, **8** No 1, 2004, 1-22.

[9] Wu, Z., Stårner, S.H., Bilger, R.W., *Proceedings of 2003 Australian Symposium on Combustion and the 8th Australian Flame Days,* Honnery, D. (Ed) (ISBN 0-7326-225124), 2003

[10] Cabra, R., http://www.me.berkeley.edu/cal/VCB/

[11] Dunn, M. J., Masri, A. R., Bilger, R. W. *Fourth Australian Conference on Laser Diagnostics in Fluid Dynamics and Combustion* To appear, 2005.

[12] Goodwin, D.G., (2003) In editor Allendorf, M., Maury, & Teyssandier, F., *Proc. CVD XVI and EuroCVD Fourteeth*.

[13] Daily J.W. (1997) *Progress in Energy and Combustion Science*, **23**, 133-199.